Bending-Shear Interaction of Cold-Formed Stainless Steel Lipped Channel Sections

D. M. M. P. Dissanayake
Faculty of Engineering and Environment, University of Northumbria,
Newcastle, UK.
K. Poologanathan
Faculty of Engineering and Environment, University of Northumbria,
Newcastle, UK.
S. Gunalan
School of Engineering and Built Environment, Griffith University,
Gold Coast, Australia.
K. D. Tsavdaridis
School of Civil Engineering, Faculty of Engineering and Physical Sciences, University of Leeds, UK.
K. S. Wanniarachchi
Faculty of Engineering, University of Ruhuna, Sri Lanka.
B. Nagaratnam
Faculty of Engineering and Environment, University of Northumbria,
Newcastle, UK.

Abstract

The bending-shear interaction response of cold-formed stainless steel lipped channel sections has been given inadequate attention in the past. Therefore, this paper investigates the bending and shear interaction behaviour of cold-formed stainless steel lipped channel sections using numerical studies. Finite element (FE) models were developed and validated against the experimental results found in the literature for three-point and four-point loading tests of lipped channel sections of both cold-formed stainless steel and cold-formed steel. The elaborated FE results were used for a comprehensive parametric study that was conducted comprising 60 FE models of three-point loading simulations of stainless steel lipped channels with five different aspect ratios to study the shear response and the bending-shear interaction response. Another 12 FE models of four-point bending simulations were developed to study the bending response.

The numerical results were analysed and it was found that the sections with aspect ratios of 1.5 and 2.0 are subjected to the interaction of bending and shear while there is no interaction effect observed in the sections with other aspect ratios. Eurocode 3 and American specifications interaction equations were then evaluated using the numerical results. These design provisions are found to be too conservative for a higher level of applied shear force. Therefore, revised design equations for bending and shear interaction were proposed aiming better prediction accuracy. Further, a statistical evaluation was conducted for the proposed interaction equations and results suggested improved and consistent predictions.

Keywords: Lipped channel beams, Cold-formed stainless steel, Bending-shear interaction, Numerical modelling, Eurocode 3, American specifications, Design rules

1 Introduction

Lipped channel beam (LCB) sections have commonly been used as load-bearing components such as roof purlins, wall studs, and floor joists in the structural applications. In practice, a higher level of stresses is developed within the cross-sections, due to the interaction of the bending and shear actions prevalent, in particular, at the supports of continuous spans and cantilever beams. The bending and shear resistances of a section tend to reduce under the bending-shear interaction, thus it is worth investigating this bending-shear interaction in the structural design process. The interaction of the bending and shear actions of hot-rolled, plate girder and cold-formed sections has been the motive for a number of investigations conducted over the years. The initial experiments on stainless steel plate girders have been performed by Olsson [1] while Real et al. [2] conducted both testing and numerical modelling of stainless steel plate girders to study the shear response. The bending-shear interaction behaviour of stainless steel plate girders have been investigated by Saliba and Gardner [3] and Chen et al. [4] using experimental and numerical studies. Sinur and Beg [5],[6] have also carried out both experimental and numerical studies on stiffened carbon steel plate girders. In addition, a number of studies have been performed on cold-formed steel sections. Keerthan and Mahendran [7] experimented the bending-shear interaction behaviour of cold-formed steel lipped channel sections, while, Pham and Hancock [8] performed both experimental and numerical studies. Furthermore, the bending-shear interaction behaviour of cold-formed steel hollow flange channel sections has been studied by Keerthan et al. [9]. However, no comprehensive investigation has been conducted for cold-formed stainless steel lipped channel

sections in the context of bending and shear interaction behaviour. Therefore, this gap in the literature was covered in this study.

Most of the design provisions for bending-shear interaction have been based on the resistance model first proposed by Basler [10]. Basler [10] investigated the bending-shear interaction of longitudinally unstiffened plate girders with slender webs and proposed a mechanical model considering the effect of interaction. This model includes the post-buckling effects of slender webs and is given by Eq. (1).

$$\left(\frac{V}{V_w}\right)^2 + \frac{M-M_f}{M_p-M_f} = 1 \text{ for } M_f < M < M_{eff} \quad (1)$$

where V_w is the web shear capacity, M_f is the bending capacity of flanges alone, M_p is the plastic bending capacity of the whole section, M_{eff} is the bending capacity of the effective cross-section, and V and M are the design shear force and design bending moment, respectively.

In this resistance model for bending-shear interaction, it is assumed that when the applied bending moment is less than the flange bending resistance, the applied bending moment is resisted solely by the flanges, therefore, no reduction occurs in the shear capacity of the webs. However, when the sections are subjected to higher moments than the flange bending resistance, a part of the section moment is transferred to the section webs and therefore, the web shear resistance begins to reduce. Thus, the interaction of bending and shear actions has to be considered.

In the current version of European standards for stainless steel (EN1993-1-4 [11]), no provisions have been made for the bending and shear interaction. This is because, EN1993-1-4 [11] provides only the supplementary provisions for stainless steel and therefore, European standards for cold-formed steel (EN1993-1-3 [12]) and European standards for plated steel (EN1993-1-5 [13]) are to be referred for the bending and shear interaction design of stainless steel cold-formed and plated sections, respectively. These interaction provisions are based on a modified version of Basler's [10] resistance model.

Bleich [14] has investigated the bending-shear interaction response of rectangular plates and proposed a circular interaction equation. This is expressed in Eq. (2). This was found to be conservative for sections with transverse stiffeners. Therefore, Shahabian and Roberts [15] have suggested a rounded interaction equation and is given by Eq. (3). Moreover, LaBoube and

Yu [16] have conducted experiments on the bending-shear interaction behaviour of cold-formed steel lipped channel sections without transverse stiffeners. Based on their work, LaBoube and Yu [16] have also proposed a relationship for the bending-shear interaction. Modified versions of some of these interaction equations have been the basis for the bending and shear interaction design provisions in American specifications for cold-formed stainless steel design, SEI/ASCE 8–02 [17].

$$\left(\frac{M}{M_n}\right)^2 + \left(\frac{V}{V_n}\right)^2 \leq 1.0 \quad (2)$$

$$\left(\frac{M}{M_n}\right)^4 + \left(\frac{V}{V_n}\right)^4 \leq 1.0 \quad (3)$$

where M_n and V_n are nominal bending strength and nominal shear strength of the section, respectively.

This paper presents the details of numerical investigations carried out to study the bending-shear interaction behaviour of cold-formed stainless steel lipped channel sections. First, a summary of codified design provisions for bending-shear interaction is discussed. Then, the details of developing the finite element (FE) models and the validation study are outlined. Thereafter, the results of the comprehensive parametric study conducted are presented. Finally, the analysis of numerical results, assessment of available design provisions, and suggested modifications to them in the context of bending-shear interaction of stainless steel LCBs are elaborated.

2 Review of design rules

In this section, design provisions for bending and shear interaction found in European standards and American specifications are discussed.

2.1 Eurocode 3 design provisions

In the absence of provisions for bending and shear interaction, European standards for stainless steel (EN1993-1-4 [11]) refers to the provisions given in European standards for cold-formed steel (EN1993-1-3 [12]) for the bending-shear interaction design of stainless steel cold-formed sections. Interaction equation provided in EN1993-1-3 [12] is based on Basler's [10] resistance model and is given by Eq. (4). This interaction model is valid only when the applied shear force (V_{Ed}) is greater than 50 % of the web shear resistance ($V_{w,Rd}$) and when the applied moment

($M_{y,Ed}$) exceeds the bending resistance corresponding to the effective areas of flanges alone ($M_{f,Rd}$).

$$\frac{M_{y,Ed}}{M_{y,Rd}} + \left(1 - \frac{M_{f,Rd}}{M_{pl,Rd}}\right)\left(\frac{2V_{Ed}}{V_{w,Rd}} - 1\right)^2 \leq 1.0 \quad (4)$$

where $M_{y,Rd}$ is the bending resistance and $M_{pl,Rd}$ is the plastic bending resistance of the section.

For the calculation of bending resistance consisting of the effective flange area ($M_{f,Rd}$) and the plastic bending resistance of the section ($M_{pl,Rd}$), provisions given in EN1993-1-5 [13] should be referred. This includes the calculation of the effective widths of plate elements according to the effective width method to account for the loss of effectiveness due to the local buckling. The cross-section bending resistance ($M_{y,Rd}$) can be calculated using Eq. (5) based on effective cross-section properties according to EN1993-1-4 [11].

$$M_{y,Rd} = M_{eff,Rd} = \frac{W_{y,eff} f_y}{\gamma_{M0}} \quad (5)$$

where $W_{y,eff}$ is the effective section modulus, f_y is the yield strength, and γ_{M0} is the partial factor for cross section resistance.

The rotated stress field theory proposed by Höglund [18] has been adopted in European standards for stainless steel (EN1993-1-4 [11]) to calculate section shear resistance. However, for the bending-shear interaction calculation, only the web contribution to shear resistance ($V_{w,Rd}$) is considered and this is given by Eq. (6).

$$V_{w,Rd} = \frac{\chi_w f_{yw} h_w t_w}{\sqrt{3}\gamma_{M1}} \quad (6)$$

where χ_w is the web shear buckling reduction factor which is a function of web slenderness ($\bar{\lambda}_w$), f_{yw} is the yield strength, h_w is the web height, t_w is the web thickness, and γ_{M1} is the partial factor for member resistance. Table 1 gives the set of equations provided in EN1993-1-4 [11] for the web shear buckling reduction factor (χ_w) of the sections with rigid end posts. Dissanayake et al. [19] has modified this set of expressions for web shear buckling reduction factor (χ_w) considering cold-formed stainless steel lipped channel sections and those are given in Table 2.

Table 1 Web shear buckling reduction factor (χ_w) of EN1993-1-4 [11] for the sections with rigid end post.

	χ_w
$\bar{\lambda}_w \leq 0.65/\eta$	η
$0.65/\eta < \bar{\lambda}_w < 0.65$	$0.65/\bar{\lambda}_w$
$\bar{\lambda}_w \geq 0.65$	$1.56/(0.91 + \bar{\lambda}_w)$

Table 2 Proposed expressions of web shear buckling reduction factor (χ_w) for the sections with rigid end post by Dissanayake et al. [19].

	χ_w
$\bar{\lambda}_w \leq 0.12$	2.1
$0.12 < \bar{\lambda}_w < 0.667$	$0.839/\bar{\lambda}_w^{\,0.433}$
$\bar{\lambda}_w \geq 0.667$	$1.797/(1.13 + \bar{\lambda}_w)$

2.2 American specifications, SEI/ASCE 8–02

In American specifications for cold-formed stainless steel (SEI/ASCE 8–02 [17]), two separate equations have been provided for the bending-shear interaction, which are for sections with and without transverse stiffeners. From Eq. (7), SEI/ASCE 8–02 [17] provision for sections with transverse stiffeners is given and this takes into account the bending-shear interaction when the applied bending moment (M) exceeds half of the section nominal moment capacity (M_n) and when the applied shear force (V) is greater than 70 % of the section nominal shear capacity (V_n).

$$0.6\left(\frac{M}{M_n}\right) + \left(\frac{V}{V_n}\right) \leq 1.3 \text{ for } \frac{M}{M_n} > 0.5 \text{ and } \frac{V}{V_n} > 0.7 \quad (7)$$

For the calculation of nominal capacities, the direct strength method (DSM) can be incorporated. The nominal bending strength for local buckling (M_{nl}) from AISI S100 [20] can be used to determine the nominal bending strength (M_n) and is expressed in Eqs. (8) and (9).

$$M_{nl} = M_{ne} \text{ for } \lambda_l \leq 0.776 \quad (8)$$

$$M_{nl} = \left[1 - 0.15\left(\frac{M_{crl}}{M_{ne}}\right)^{0.4}\right]\left(\frac{M_{crl}}{M_{ne}}\right)^{0.4} M_{ne} \text{ for } \lambda_l > 0.776 \quad (9)$$

where M_{ne} is the critical elastic lateral-torsional buckling moment, M_{crl} is the critical elastic local buckling moment, and λ_l is the section slenderness.

The nominal shear strength (V_n) can be calculated from AISI S100 [20] using Eqs. (10) and (11).

$$V_n = V_y \text{ for } \lambda_v \leq 0.776 \quad (10)$$

$$V_n = \left[1 - 0.15\left(\frac{V_{cr}}{V_y}\right)^{0.4}\right]\left(\frac{V_{cr}}{V_y}\right)^{0.4} V_y \text{ for } \lambda_v > 0.776 \quad (11)$$

where V_y is the shear yield force, V_{cr} is the elastic shear buckling force, and λ_v is the section slenderness.

Dissanayake et al. [19] also proposed modified set of equations to determine the shear strength of cold-formed stainless steel lipped channel sections using DSM and these DSM provisions are expressed in Eqs. (12)-(14).

$$V_n = 2V_y \text{ for } \lambda_v \leq 0.122 \quad (12)$$

$$V_n = \frac{0.795}{\lambda_v^{0.439}} V_y \text{ for } 0.122 < \lambda_v \leq 0.592 \quad (13)$$

$$V_n = \left[1 - 0.213\left(\frac{V_{cr}}{V_y}\right)^{0.35}\right]\left(\frac{V_{cr}}{V_y}\right)^{0.35} V_y \text{ for } \lambda_v > 0.592 \quad (14)$$

In addition to this linear interaction equation, a circular interaction equation is also provided in SEI/ASCE 8–02 [17] for sections without transverse stiffeners and this is similar to the expression given in Eq. (2).

3 Finite element (FE) modelling

Commercially available ABAQUS CAE 2017 software package was employed to develop the FE models to investigate the bending and shear interaction behaviour of cold-formed stainless steel lipped channel sections. The details of numerical simulations carried out are similar to the numerical modelling out lined in Dissanayake et al. [19] and are summarised in this section.

3.1 General

Three-point loading tests of LCBs found from [7],[19] were simulated in ABAQUS to study the bending-shear interaction. To avoid any torsional effects on the structural behaviour of LCBs, back-to-back beam setup has been employed by attaching two LCBs from their webs in the experiments. Simply supported boundary conditions and mid-span loading have been assigned to the sections through hot-rolled T-stiffeners. The T-stiffeners have been bolted to two LCBs using web side plates to avoid any web bearing failure. Both top and bottom flanges have been restrained against distortional buckling by screwing equal angle (EA) straps to them at the loading point and at two supports. More details of these three-point loading tests can be found in [7],[19],[21]–[23]. However, considering the symmetry of the test setup, single LCBs were simulated with three web side plates in the FE models developed in this study. The schematic diagram of three-point loading test setup and cross-sectional dimensions of a LCB section are shown in Fig. 1. In the FE modelling, the shear behaviour and the bending-shear interaction behaviour of LCBs were simulated using this setup.

In addition, it was required to study the bending behaviour of LCBs to find out their bending capacities. For this purpose, four-point bending test setup given in [8] was utilised and then FE models were developed for each cross-section considered in this study. More details of four-point bending tests can be found in [8],[24].

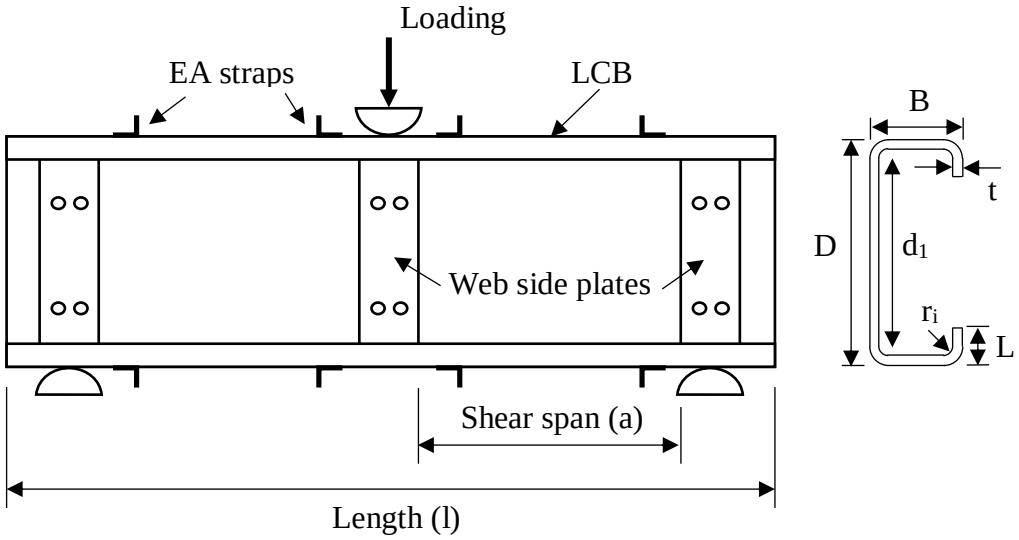

Fig. 1 Schematic diagram of three-point loading arrangement and cross-sectional dimensions

3.2 Element type and mesh

The four-node shell element type known as S4R was chosen from ABAQUS element library to model both LCB sections and web side plates. These S4R shell elements have six degrees of freedom (DOFs) at each node. Mesh sensitivity analysis suggested that the assigning of 5 mm × 5 mm mesh for flat parts of LCB sections and assigning of a relatively finer mesh of 1 mm × 5 mm for corner regions of LCB sections are sufficient. However, as web side plates are less important, a comparatively coarser mesh of 10 mm × 10 mm was used for modelling them. Fig. 2 illustrates the assembly of parts together with the FE mesh assigned in the modelling.

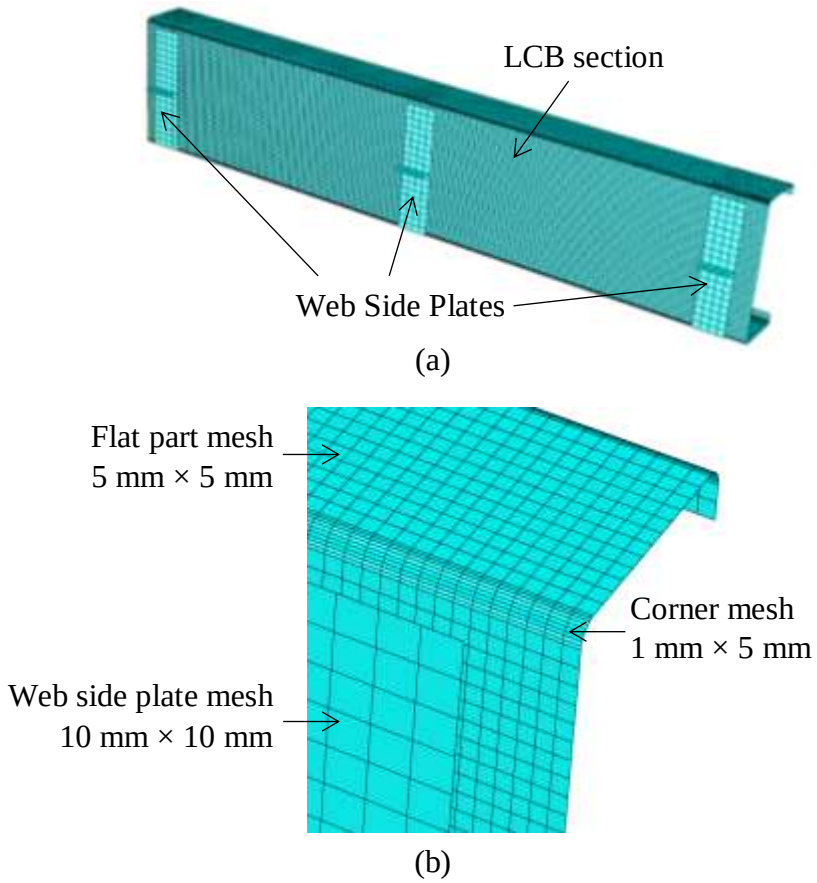

Fig. 2 (a) Assembly of parts and (b) FE mesh used in the modelling

3.3 Material modelling of stainless steel

Arrayago et al. [25] have recently proposed modifications to the two-stage Ramberg-Osgood material model. The modified two-stage Ramberg-Osgood material model with these recent proposals was incorporated in calculating stress-strain data for stainless steel in this study. Then, true stress (σ_{true}) and log plastic strain (ε_{ln}^{pl}) data of the non-linear material was inputted

into ABAQUS. The true stress (σ_{true}) and log plastic strain (ε_{ln}^{pl}) were calculated using Eqs. (15) and (16), respectively. The strength enhancements induced during the press-braking process of LCB sections were introduced to the corner regions as described in [19]. For the FE modelling of carbon steel sections, an elastic, perfectly-plastic material model was employed. The incorporated material models are illustrated in Fig. 3.

$$\sigma_{true} = \sigma_{nom}(1 + \varepsilon_{nom}) \quad (15)$$

$$\varepsilon_{ln}^{pl} = \ln(1 + \varepsilon_{nom}) - \frac{\sigma_{true}}{E} \quad (16)$$

where σ_{nom} is the engineering stress, ε_{nom} is the engineering strain, and E is Young's modulus.

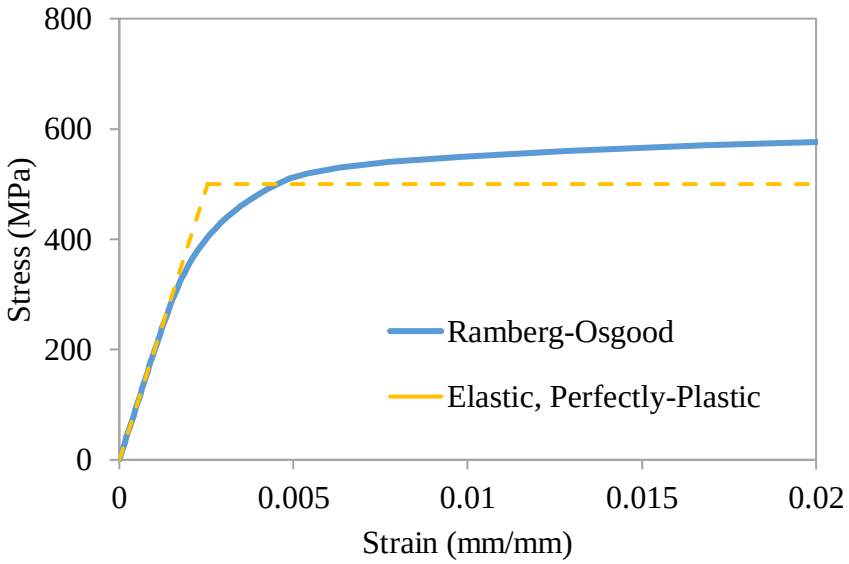

Fig. 3 Different material models used in the FE modelling

During the section forming, two types of residual stresses are formed in press-braked sections and these are known as bending and membrane residual stresses. The bending residual stresses are indirectly accounted in material stress-strain data while membrane residual stresses are found to be negligible for press-braked sections [26]. The similar numerical studies have also ignored the residual stresses arising from the section forming in the numerical modelling as these residual stresses have very small effect [26],[27]. Therefore, the effect of these residual stresses were not explicitly considered in the FE modelling of this study.

3.4 Boundary conditions

The boundary conditions were chosen as they accurately simulate the experimental conditions. All three translational DOFs were restrained at one end to maintain a pin support condition while only the translational DOFs in the cross-sectional plane were restrained at the other end to maintain a roller support condition. To avoid any rotation of the section, the rotational DOF about the longitudinal axis was restrained at both supports. The loading was given at the mid-span by applying a vertical displacement. The loading and the support conditions were assigned to web side plates to suppress any web bearing failure at these locations. The translational DOF in the transverse direction and the rotational DOF about the longitudinal axis were restrained at the EA strap locations to eliminate distortional buckling. To simulate bolted connections between LCB web and web side plates, tie constraints (available in ABAQUS) were assigned. The locations of the assigned boundary conditions in the FE modelling are given in Fig. 4.

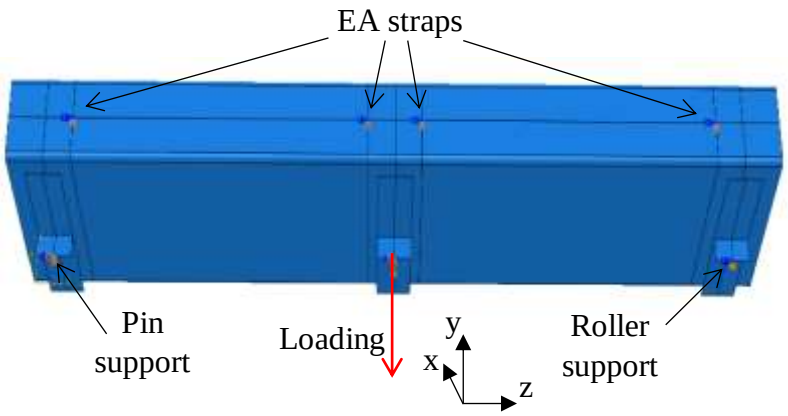

Fig. 4 The locations of the boundary conditions assigned in the FE modelling

3.5 Analysis methods

To account for geometric imperfections in the non-linear analysis, first, an Eigenvalue buckling analysis was conducted on the perfect geometry. Then, the critical buckling Eigenmode shapes were extracted from the analysis. The web shear buckling mode with the lowest Eigenvalue was chosen from each analysis. Thereafter, these critical mode shapes were superimposed on to the non-linear FE models using a suitable scale factor which represents the magnitude of imperfections. In this study, the modified Dawson and Walker model proposed by Gardner and Nethercot [28] was used as the imperfection amplitude (ω_0). The modified Dawson and Walker model is given by Eq. (17).

$$\omega_0 = 0.023\left(\frac{\sigma_{0.2}}{\sigma_{cr}}\right)t \quad (17)$$

where $\sigma_{0.2}$ is the 0.2 % proof stress of the material, σ_{cr} is the critical elastic buckling stress of the most slender element of the section, and t is the thickness.

Secondly, a modified static Riks analysis was performed on the geometrically and materially non-linear FE models until the failure occurs, to study the section behaviour. More details related to FE modelling of cold-formed channel sections can be found from [29]–[31].

4 Validation of FE models

Comparisons of the FE results obtained from the developed models were compared with the experimental results found from the literature and those details are given in this section. The shear, bending, and bending-shear interaction tests were covered in this validation process.

In this paper, LCB cross-sections are denoted as LCB D × B × L × t. This notation stands for key cross-sectional dimensions in millimetres where D is the section depth, B is the flange width, L is the lip height, and t is the section thickness. These cross-sectional dimensions are defined in Fig. 1.

4.1 Shear behaviour

Dissanayake et al. [19] have investigated the shear behaviour of cold-formed stainless steel LCBs using three-point loading tests. These experimental results are compared with the FE results in Table 3 for the validation of FE modelling for shear behaviour. The section length and the shear span length for each section are also given in Table 3. The shear span (a) to clear web depth (d_1) ratio is taken as the aspect ratio of the specimen and the definition of these parameters are illustrated in Fig.1. The shear capacity of a section is independent of its bending stresses when shorter spans (such as sections with an aspect ratio of 1.0) are employed while the bending-shear interaction is taken place when longer spans are employed [7]. Therefore, all the compared sections have an aspect ratio of 1.0. From the comparisons, it can be seen that the mean and the coefficient of variation (COV) of experimental to FE shear capacity ratio are 1.02 and 0.073, respectively. This confirms the ability of developed FE models to predict the shear capacities of cold-formed stainless steel LCBs with good accuracy. Additionally, Fig. 5 compares the experimental and FE shear failure modes for LCB 200×75×15×1.2 section. It can be concluded from Fig. 5, that the developed FE models are able to accurately capture the

diagonal shear failures of LCB webs as well. The experimental and FE load-deflection curves of LCB 150×65×15×2.0 section are also compared in Fig. 6. The slip between the plates and specimens at the bolted connections could be the reason for higher deflections in the experiments compared to FE results.

Table 3 Comparison of experimental [19] and FE section capacities for stainless steel LCBs subjected to shear

LCB section	l (mm)	a (mm)	$\bar{\lambda}_w$	$V_{Exp.}$ (kN)	V_{FE} (kN)	$\frac{V_{Exp.}}{V_{FE}}$
LCB 100×50×15×1.2	380	97.5	0.78	18.49	16.86	1.10
LCB 100×50×15×1.5	379	97.0	0.61	24.44	23.90	1.02
LCB 100×50×15×2.0	376	95.5	0.45	36.00	32.72	1.10
LCB 150×65×15×1.2	479	147.0	1.17	21.60	20.09	1.08
LCB 150×65×15×1.5	479	147.0	0.92	26.26	28.40	0.92
LCB 150×65×15×2.0	478	146.5	0.69	43.55	42.60	1.02
LCB 200×75×15×1.2	579	197.0	1.57	22.98	22.97	1.00
LCB 200×75×15×2.0	579	197.0	0.93	47.05	52.11	0.90
Mean						1.02
COV						0.073

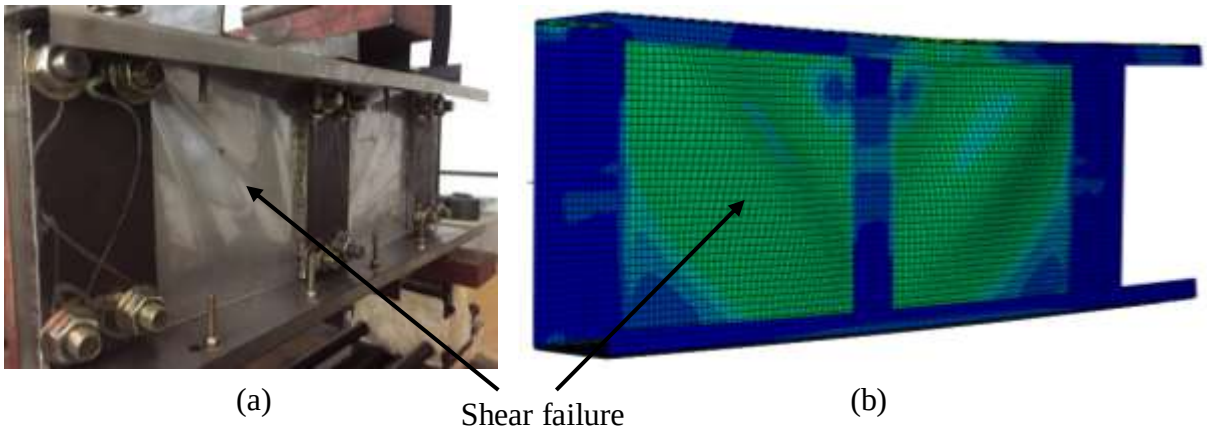

Fig. 5 (a) Experimental [19] and (b) FE failure modes of stainless steel LCB 200×75×15×1.2 section subjected to shear

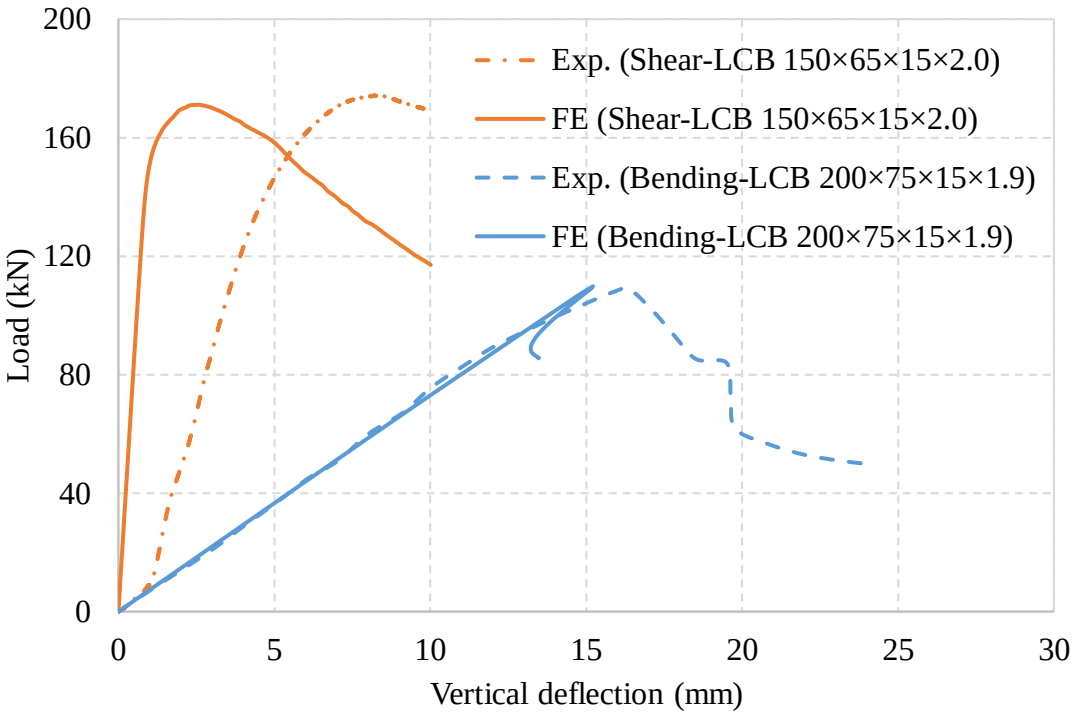

Fig. 6 Comparison of experimental and FE load-deflection curves

4.2 Bending behaviour

To study the bending behaviour, four-point bending tests of cold-formed steel LCB sections found from Pham and Hancock [8] were simulated in ABAQUS. A specimen length of 2695 mm was utilised in the FE modelling according to bending tests conducted by Pham and Hancock [8]. In the FE modelling, an elastic, perfectly-plastic material model was employed for cold-formed steel, with no consideration given to corner strength enhancements. Experimental and FE ultimate loads of four-point bending tests of cold-formed steel LCB sections are compared in Table 4. In Table 4, P is the ultimate load. The experimental to FE ultimate load ratio has a mean and a COV of 1.02 and 0.056, respectively. Therefore, good accuracy of capacity predictions is evident from the comparisons. In addition, comparisons are made between experimental and FE failure modes in Fig. 7 and experimental and FE load-deflection curves in Fig. 6 for LCB 200×75×15×1.9 section. Both these comparisons show good agreement as well. Therefore, the elaborated FE models can be utilised to study the bending response of cold-formed stainless steel LCB sections.

Table 4 Comparison of experimental [8] and FE section capacities for cold-formed steel LCBs subjected to bending

LCB section	$P_{Exp.}$ (kN)	$M_{Exp.}$ (kNm)	P_{FE} (kN)	M_{FE} (kNm)	$\frac{P_{Exp.}}{P_{FE}}$
LCB 150×65×15×1.5	52.13	10.43	53.64	10.73	0.97
LCB 150×65×15×2.4	99.19	19.84	90.04	18.01	1.10
LCB 200×75×15×1.5	67.33	13.47	66.00	13.20	1.02
LCB 200×75×15×1.9	108.78	21.76	109.80	21.96	0.99
Mean					1.02
COV					0.056

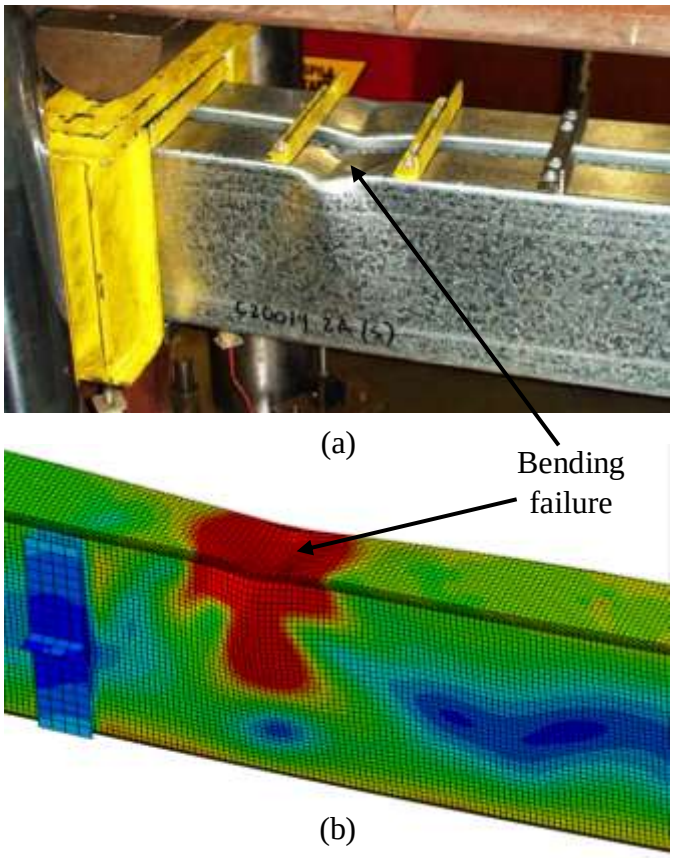

(a)

(b)

Fig. 7 (a) Experimental [8] and (b) FE failure modes of cold-formed steel LCB 200×75×15×1.9 section subjected to bending

4.3 Bending-shear interaction behaviour

Keerthan and Mahendran [7] have investigated the bending-shear interaction behaviour of cold-formed steel LCB sections with an aspect ratio (a/d_1) of 1.5 using three-point loading tests. These tests were simulated in the FE modelling and results were compared. Table 5 summarises the experimental and FE capacities. From the comparisons, it can be seen that the experimental to FE shear capacity ratio has a mean of 1.01 and a COV of 0.067. Therefore, the capacity prediction accuracy of the FE models is highlighted for higher aspect ratios as well. Moreover, good agreement can be seen between experimental and FE bending-shear interaction failure modes for LCB 250×75×18×1.9 section in Fig. 8.

Table 5 Comparison of experimental [7] and FE section capacities for cold-formed steel LCBs subjected to bending-shear interaction

LCB section	l (mm)	a (mm)	$\bar{\lambda}_w$	$V_{Exp.}$ (kN)	$M_{Exp.}$ (kNm)	V_{FE} (kN)	M_{FE} (kNm)	$\frac{V_{Exp.}}{V_{FE}}$ or $\frac{M_{Exp.}}{M_{FE}}$
LCB 160×65×15×1.5	654	156.4	1.61	39.70	9.31	38.77	9.10	1.02
LCB 160×65×15×1.9	659	158.0	1.26	56.80	13.46	53.50	12.68	1.06
LCB 200×75×15×1.5	775	196.8	2.05	38.10	11.25	41.30	12.19	0.92
LCB 200×75×15×1.9	776	197.0	1.58	56.91	16.82	58.77	17.37	0.97
LCB 200×75×15×1.95	776	197.0	1.12	39.51	11.68	36.38	10.75	1.09
LCB 250×75×18×1.5	927	247.2	2.56	42.90	15.91	44.50	16.50	0.96
LCB 250×75×18×1.9	927	247.3	1.98	60.70	22.52	64.28	23.84	0.94
LCB 250×75×18×1.95	929	248.0	1.41	44.37	16.51	40.55	15.08	1.09
Mean								1.01
COV								0.067

(a)

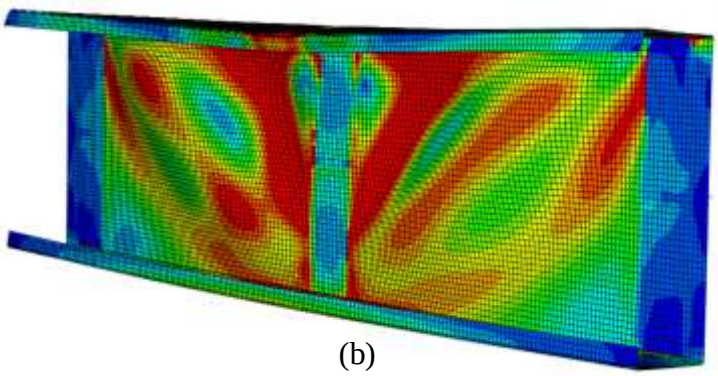

(b)

Fig. 8 (a) Experimental [7] and (b) FE failure modes of cold-formed steel LCB 250×75×18×1.9 section subjected to bending-shear interaction

5 Numerical parametric study

5.1 General

A comprehensive parametric study was conducted to generate a numerical database covering a wider area of different parameters following the successful validation of developed FE models. Then, this numerical data was utilised to investigate the bending and shear interaction behaviour of cold-formed stainless steel LCBs.

Three scenarios were considered in the study. The validated FE models of three-point loading tests with shorter spans (in Section 4.1) were utilised to simulate the shear behaviour while the validated FE models of three-point loading tests with longer spans (in Section 4.3) were considered to simulate the bending-shear interaction behaviour. In addition, the validated FE models of four-point bending tests (in Section 4.2) were incorporated to simulate the bending behaviour and to find out the bending capacities of varying LCB sections considered in the parametric study. Altogether 12 different cross sections were considered with two section depths (D), three section thicknesses (t) and two stainless steel grades. To vary the level of

bending-shear interaction, a total of 48 FE models were developed with four different aspect ratio (a/d_1) values. Table 6 summarises these parameters used in the study.

Table 6 Summary of the parameters considered in the study

Scenario	Sections	a/d_1	l (mm)	t (mm)	Stainless steel grade	No. of models
1. Four-point bending simulation	LCB 150×65×15×t LCB 200×75×20×t	-	2695	1 1.5 2	Austenitic-1.4301 Duplex-1.4462	12
2. Three-point loading simulation with shorter spans	LCB 150×65×15×t	1	485	1	Austenitic-1.4301	12
	LCB 200×75×20×t	1	585	1.5 2	Duplex-1.4462	
3. Three-point loading simulation with longer spans	LCB 150×65×15×t	1.5	635	1	Austenitic-1.4301	48
		2	785	1.5	Duplex-1.4462	
		3	1085	2		
		5	1685			
	LCB 200×75×20×t	1.5	785			
		2	985			
		3	1385			
		5	2185			

Both austenitic and duplex stainless steel grades were considered in the study and Table 7 brief the basic material properties employed in the FE models where f_y is the yield stress, f_u is the ultimate stress, ε_u is the ultimate strain, and n and m are Ramberg-Osgood parameters. The yield stress (f_y) and the ultimate stress (f_u) values for each stainless steel grade were taken from EN1993-1-4 [11] and the recommendations of Arrayago et al. [25] were adopted for the ultimate strain (ε_u) and Ramberg-Osgood parameters. Young's modulus was taken as 200,000 MPa and a value of 0.3 was used for Poisson's ratio. The stress-strain relationships of two stainless steel grades considered are illustrated in Fig. 9.

Table 7 Material properties used in the parametric study

Stainless steel grade	f_y (MPa)	f_u (MPa)	ε_u	n	m
Austenitic-1.4301	230	540	0.57	7	2.19
Duplex-1.4462	500	700	0.29	8	3.00

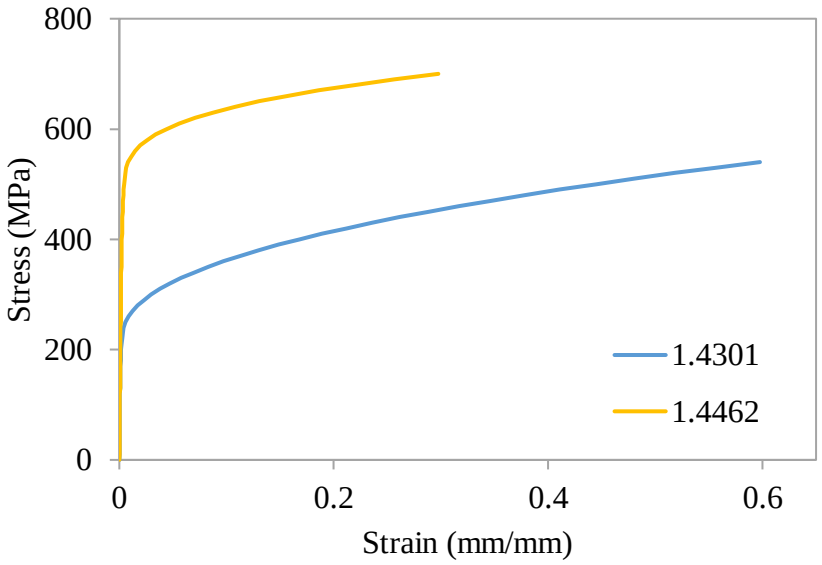

Fig. 9 Stress-strain curves for 1.4301 and 1.4462 stainless steel grades

5.2 Comparison of FE results with Eurocode 3 and the DSM predictions

The numerical parametric study results are summarised in this section. Table 8 compares the cross-sectional bending capacities ($M_{u,FE}$) found from the FE simulations of four-point bending setup (Scenario 1 in Table 6) with the Eurocode 3 predictions of moment resistance (M_{EC3}) and the DSM predictions of moment capacity (M_{DSM}). In Table 8, M_{EC3} was calculated from Eq. (5) while M_{DSM} was evaluated from Eqs. (8) and (9). From the mean and the COV of FE to predicted capacity ratio, it can be concluded that the code predictions are too conservative for cold-formed stainless steel LCBs. Therefore, the numerical values of cross-section bending resistance ($M_{u,FE}$) were adopted in the evaluation of bending-shear interaction equations in Section 6.

386 Table 8 Numerical parametric study results of Scenario 1

LCB section	$M_{u,FE}$ (kNm)	M_{EC3} (kNm)	M_{DSM} (kNm)	$\frac{M_{u,FE}}{M_{EC3}}$	$\frac{M_{u,FE}}{M_{DSM}}$
Stainless steel grade 1.4301					
LCB 150×65×15×1.0	3.06	2.34	2.73	1.30	1.12
LCB 150×65×15×1.5	5.75	4.55	4.95	1.26	1.16
LCB 150×65×15×2.0	8.05	6.43	6.48	1.25	1.24
LCB 200×75×20×1.0	4.30	3.33	3.85	1.29	1.11
LCB 200×75×20×1.5	8.72	6.60	7.50	1.32	1.16
LCB 200×75×20×2.0	12.80	10.41	10.72	1.23	1.19
Stainless steel grade 1.4462					
LCB 150×65×15×1.0	4.98	3.81	4.54	1.31	1.10
LCB 150×65×15×1.5	10.06	7.64	8.86	1.32	1.14
LCB 150×65×15×2.0	15.24	12.20	13.99	1.25	1.09
LCB 200×75×20×1.0	6.85	5.34	6.36	1.28	1.08
LCB 200×75×20×1.5	13.78	10.92	12.58	1.26	1.10
LCB 200×75×20×2.0	23.26	17.75	20.12	1.31	1.16
Mean				1.28	1.14
COV				0.024	0.043

387

388 The parametric study results of FE simulations of three-point loading setup for a/d_1=1.0
389 (Scenario 2 in Table 6) are summarised in Table 9 while Tables 10-13 provide that of the
390 sections with longer spans (Scenario 3 in Table 6). In Tables 9-13, V and M are the numerical
391 values of the shear force and the bending moment at the failure of the section, respectively.
392 $V_{EC3,[19]}$ is the shear resistance of the section according to Eurocode 3 for stainless steel
393 calculated from Eq. (6) where modified expressions for shear buckling reduction factor from
394 [19] (using Table 2) were incorporated. $V_{DSM,\,[19]}$ is the DSM shear capacity of the section
395 calculated from Eqs. (12)-(14).

396 The mean and the COV of FE to predicted shear capacity ratio given in Table 9 suggest that
397 the numerical shear capacities are agree well with the shear capacity predictions. Therefore,

this confirms that the shear capacity of the section is not affected by the bending moment when shorter spans (a/d_1=1.0) are employed. In addition, the bending moment of the section (M) is compared with the bending resistance consisting of the effective flange area ($M_{f,Rd}$) in Table 9. This comparison suggests that even though the section moment (M) is as high as $1.3 \times M_{f,Rd}$, the shear capacity (V) of the section is not reduced.

Further, the progressive reduction of the section shear force (V) compared to the section shear resistance is observed with the increment of the section bending moment (M) compared to the section bending resistance from Tables 10-13. This confirms that the numerically obtained shear capacities of the sections with longer spans are not independent of bending stresses of the section. Therefore, the shear provisions given in Section 2 were utilised to calculate the shear resistances of sections when evaluating the bending-shear interaction equations in Section 6. However, no reduction in section bending moment (M) can be observed for sections with aspect ratios of 3.0 and 5.0 from Tables 12 and 13.

Moreover, FE results shows that the employed duplex stainless steel grade results in higher shear forces and bending moments in the sections than austenitic stainless steel grade. However, no clear difference was observed in the interaction behaviour of the sections of these two stainless steel grades from the numerical results of the parametric study.

425 Table 9 Numerical parametric study results of Scenario 2 (a/d_1=1.0)

LCB section	V (kN)	M (kNm)	$V_{EC3,[19]}$ (kN)	$V_{DSM,[19]}$ (kN)	$\frac{V}{V_{EC3,[19]}}$	$\frac{V}{V_{DSM,[19]}}$	$\frac{M}{M_{u,FE}}$	$\frac{M}{M_{f,Rd}}$
Stainless steel grade 1.4301								
LCB 150×65×15×1.0	15.25	2.27	14.27	13.89	1.07	1.10	0.74	1.28
LCB 150×65×15×1.5	27.62	4.10	25.91	25.55	1.07	1.08	0.71	1.18
LCB 150×65×15×2.0	40.15	5.94	38.66	38.53	1.04	1.04	0.74	1.19
LCB 200×75×20×1.0	17.23	3.43	16.24	15.82	1.06	1.09	0.80	1.38
LCB 200×75×20×1.5	32.19	6.39	30.42	29.65	1.06	1.09	0.73	1.27
LCB 200×75×20×2.0	48.90	9.68	46.25	45.59	1.06	1.07	0.76	1.21
Stainless steel grade 1.4462								
LCB 150×65×15×1.0	25.69	3.83	24.79	24.22	1.04	1.06	0.77	1.37
LCB 150×65×15×1.5	50.58	7.51	46.82	45.56	1.08	1.11	0.75	1.30
LCB 150×65×15×2.0	76.38	11.30	71.57	70.28	1.07	1.09	0.74	1.21
LCB 200×75×20×1.0	28.21	5.61	27.44	27.29	1.03	1.03	0.82	1.47
LCB 200×75×20×1.5	57.15	11.34	53.40	51.99	1.07	1.10	0.82	1.39
LCB 200×75×20×2.0	88.82	17.59	83.51	81.25	1.06	1.09	0.76	1.30
Mean					1.06	1.08	0.76	1.30
COV					0.015	0.022	0.046	0.070

426

427

428

429

430

431

432

433

434 Table 10 Numerical parametric study results of Scenario 3 (a/d_1=1.5)

LCB section	V (kN)	M (kNm)	$V_{EC3,[19]}$ (kN)	$V_{DSM,[19]}$ (kN)	$\frac{V}{V_{EC3,[19]}}$	$\frac{V}{V_{DSM,[19]}}$	$\frac{M}{M_{u,FE}}$
Stainless steel grade 1.4301							
LCB 150×65×15×1.0	12.07	2.70	13.25	13.32	0.91	0.91	0.88
LCB 150×65×15×1.5	22.49	5.01	24.39	24.63	0.92	0.91	0.87
LCB 150×65×15×2.0	33.01	7.33	36.61	37.34	0.90	0.88	0.91
LCB 200×75×20×1.0	13.34	3.98	14.93	15.14	0.89	0.88	0.93
LCB 200×75×20×1.5	26.19	7.80	28.34	28.48	0.92	0.92	0.89
LCB 200×75×20×2.0	39.69	11.79	43.52	43.94	0.91	0.90	0.92
Stainless steel grade 1.4462							
LCB 150×65×15×1.0	19.18	4.29	22.73	23.16	0.84	0.83	0.86
LCB 150×65×15×1.5	39.76	8.86	43.50	43.71	0.91	0.91	0.88
LCB 150×65×15×2.0	62.30	13.83	67.16	67.66	0.93	0.92	0.91
LCB 200×75×20×1.0	20.89	6.24	24.93	26.05	0.84	0.80	0.91
LCB 200×75×20×1.5	43.73	13.02	49.12	49.75	0.89	0.88	0.94
LCB 200×75×20×2.0	71.84	21.34	77.57	77.95	0.93	0.92	0.92
Mean					0.90	0.89	0.90
COV					0.034	0.043	0.027

435

436

437

438

439

440

441

442

443 Table 11 Numerical parametric study results of Scenario 3 (a/d_1=2.0)

LCB section	V (kN)	M (kNm)	$V_{EC3,[19]}$ (kN)	$V_{DSM,[19]}$ (kN)	$\frac{V}{V_{EC3,[19]}}$	$\frac{V}{V_{DSM,[19]}}$	$\frac{M}{M_{u,FE}}$
Stainless steel grade 1.4301							
LCB 150×65×15×1.0	9.76	2.91	12.82	13.02	0.76	0.75	0.95
LCB 150×65×15×1.5	18.20	5.41	23.74	24.13	0.77	0.75	0.94
LCB 150×65×15×2.0	26.29	7.78	35.78	36.68	0.73	0.72	0.97
LCB 200×75×20×1.0	10.63	4.23	14.38	14.77	0.74	0.72	0.98
LCB 200×75×20×1.5	21.18	8.41	27.47	27.85	0.77	0.76	0.96
LCB 200×75×20×2.0	31.95	12.65	42.35	43.06	0.75	0.74	0.99
Stainless steel grade 1.4462							
LCB 150×65×15×1.0	15.26	4.55	21.87	22.60	0.70	0.68	0.91
LCB 150×65×15×1.5	32.27	9.58	42.10	42.72	0.77	0.76	0.95
LCB 150×65×15×2.0	50.04	14.81	65.28	66.25	0.77	0.76	0.97
LCB 200×75×20×1.0	16.32	6.50	23.91	25.39	0.68	0.64	0.95
LCB 200×75×20×1.5	34.73	13.79	47.34	48.56	0.73	0.72	1.00
LCB 200×75×20×2.0	58.15	23.03	75.06	76.19	0.77	0.76	0.99
Mean					0.75	0.73	0.96
COV					0.040	0.52	0.026

444

445

446

447

448

449

450

451

452 Table 12 Numerical parametric study results of Scenario 3 (a/d_1=3.0)

LCB section	V (kN)	M (kNm)	$V_{EC3,[19]}$ (kN)	$V_{DSM,[19]}$ (kN)	$\frac{V}{V_{EC3,[19]}}$	$\frac{V}{V_{DSM,[19]}}$	$\frac{M}{M_{u,FE}}$
Stainless steel grade 1.4301							
LCB 150×65×15×1.0	6.73	3.01	12.48	12.71	0.54	0.53	0.98
LCB 150×65×15×1.5	13.04	5.81	23.22	23.62	0.56	0.55	1.01
LCB 150×65×15×2.0	18.42	8.18	35.11	36.00	0.52	0.51	1.02
LCB 200×75×20×1.0	7.11	4.24	13.96	14.41	0.51	0.49	0.99
LCB 200×75×20×1.5	14.93	8.89	26.78	27.20	0.56	0.55	1.02
LCB 200×75×20×2.0	22.21	13.19	41.43	42.14	0.54	0.53	1.03
Stainless steel grade 1.4462							
LCB 150×65×15×1.0	10.18	4.55	21.20	22.03	0.48	0.46	0.91
LCB 150×65×15×1.5	22.01	9.81	41.00	41.72	0.54	0.53	0.97
LCB 150×65×15×2.0	35.39	15.71	63.78	64.80	0.55	0.55	1.03
LCB 200×75×20×1.0	10.81	6.45	23.12	24.73	0.47	0.44	0.94
LCB 200×75×20×1.5	23.33	13.89	45.95	47.36	0.51	0.49	1.01
LCB 200×75×20×2.0	40.17	23.86	73.10	74.39	0.55	0.54	1.03
Mean					0.53	0.51	1.00
COV					0.058	0.070	0.037

453

454

455

456

457

458

459

460

Table 13 Numerical parametric study results of Scenario 3 (a/d_1=5.0)

LCB section	V (kN)	M (kNm)	$V_{EC3,[19]}$ (kN)	$V_{DSM,[19]}$ (kN)	$\frac{V}{V_{EC3,[19]}}$	$\frac{V}{V_{DSM,[19]}}$	$\frac{M}{M_{u,FE}}$
Stainless steel grade 1.4301							
LCB 150×65×15×1.0	4.23	3.15	12.30	12.46	0.34	0.34	1.03
LCB 150×65×15×1.5	7.97	5.92	22.93	23.21	0.35	0.34	1.03
LCB 150×65×15×2.0	11.24	8.32	34.74	35.45	0.32	0.32	1.03
LCB 200×75×20×1.0	4.31	4.29	13.73	14.11	0.31	0.31	1.00
LCB 200×75×20×1.5	8.99	8.92	26.40	26.69	0.34	0.34	1.02
LCB 200×75×20×2.0	13.46	13.33	40.92	41.41	0.33	0.33	1.04
Stainless steel grade 1.4462							
LCB 150×65×15×1.0	6.16	4.59	20.84	21.57	0.30	0.29	0.92
LCB 150×65×15×1.5	13.65	10.14	40.40	40.91	0.34	0.33	1.01
LCB 150×65×15×2.0	21.68	16.04	62.96	63.64	0.34	0.34	1.05
LCB 200×75×20×1.0	6.64	6.61	22.69	24.20	0.29	0.27	0.96
LCB 200×75×20×1.5	13.87	13.77	45.20	46.40	0.31	0.30	1.00
LCB 200×75×20×2.0	24.20	23.96	72.02	72.96	0.34	0.33	1.03
Mean					0.33	0.32	1.01
COV					0.060	0.073	0.036

6 Results analysis

The insight into the bending and shear interaction of cold-formed stainless steel LCBs acquired from the numerical studies conducted in this paper was utilised in assessing the interaction equations discussed in Section 2 and the details are presented in this section.

6.1 Failure modes

Using the FE results obtained in the parametric study, an analysis of failure modes was conducted and the dominant failure modes of three-point loading simulations of stainless steel LCB sections for each aspect ratio were identified. Fig. 10 illustrates the identified dominant failure modes of stainless steel LCB sections together with their load-deflection curves for each

aspect ratio. From Fig. 10 (a), it can be clearly seen that the diagonal shear failure of both webs of sections with an aspect ratio of 1.0, and can be concluded that these sections fail primarily in shear, as it is expected. Figs. 10 (b) and (c) depict the dominant failure modes of sections with aspect ratios of 1.5 and 2.0, respectively. It is observed that both local buckling failure of the compression flange and diagonal shear failure of the webs occur in the sections with these two aspect ratios. Therefore, the sections with aspect ratios of 1.5 and 2.0 are subjected to the bending and shear interaction. Local buckling of the compression flange is visible from Figs. 10 (d) and (e) for the sections with aspect ratios of 3.0 and 5.0, respectively, and there is no clear sign of any web shear failure. This observation leads to the conclusion that sections with aspect ratios of 3.0 and 5.0 behave primarily in bending. In the next section, the bending-shear interaction equations discussed in Section 2 were assessed, while giving due consideration to the above findings from FE analysis conducted in this study.

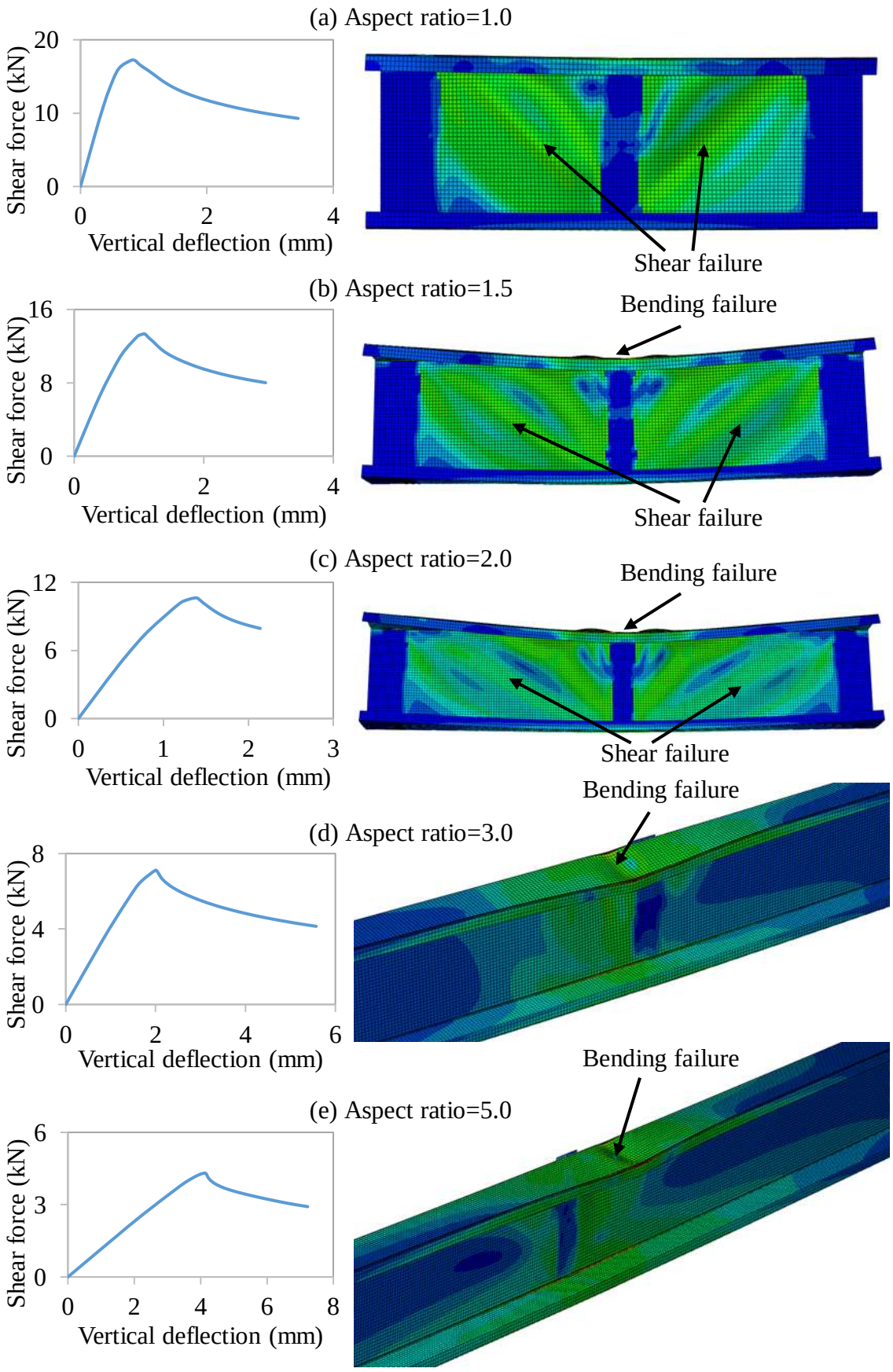

484

485 Fig. 10 Failure modes and load-deflection curves of stainless steel LCB sections for different aspect ratios

6.2 Assessment of EN1993-1-3 interaction equation

The following sections are dealing with the evaluation of codified interaction equations for the bending and shear interaction of cold-formed stainless steel LCB sections using the generated numerical results of the parametric study. For this purpose, numerical resistance values were compared with predicted resistance values. Fig. 11 illustrates the definition of the actual value of the resistance (experimental or FE) with the predicted value of the resistance from an interaction curve. The distance from the origin to the actual data point in the bending-shear interaction diagram defines the actual resistance. The distance between the origin and the intersection point of the origin to the actual data point line and the interaction curve represents the predicted resistance. If the actual data point lies outside the interaction curve, it is said to be a safe prediction and if the point lies within the curve it is said to be unsafe.

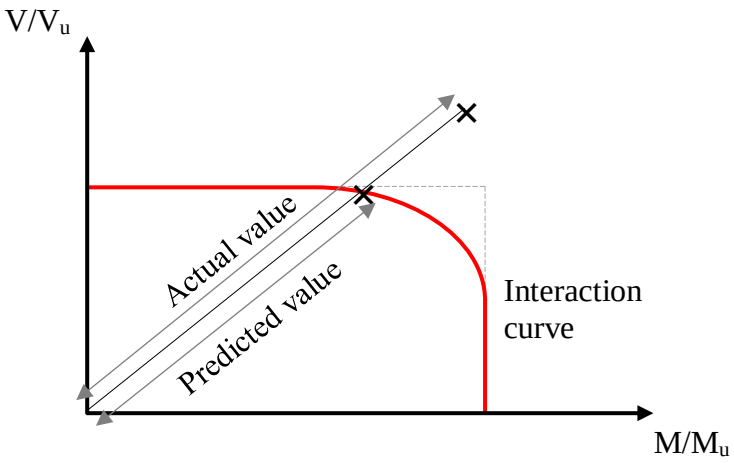

Fig. 11 Definition of actual and predicted resistances with respect to the interaction curve

Fig. 12 plots the FE results of stainless steel LCB sections given in Tables 9-13 for each aspect ratio with the bending-shear interaction curve from EN1993-1-3 [12]. It can be observed from the distribution of FE data points in the interaction diagram that LCB sections with an aspect ratio of 1.0 do not exhibit any shear capacity reduction. However, a reduction of shear capacity can be seen for the sections with aspect ratios of 1.5 and 2.0, when the bending and shear interaction effect takes place. Also, there is no evidence of bending capacity reduction in the sections with higher aspect ratios such as 3.0 and 5.0. From the comparison, it can be seen that EN1993-1-3 [12] interaction equation is able to safely predict the resistance of cold-formed stainless steel LCB sections subjected to bending and shear interaction, however, a conservative nature in predictions may exist when $V/V_{w,Rd}$ ratio is closer to 1.0. This is because, the assumption of bending-shear interaction when the applied bending moment (M) exceeds

the bending resistance of the flanges with effective flange area ($M_{f,Rd}$), seems to be not applicable for cold-formed stainless steel LCB sections. It was shown that the shear capacity of sections with shorter spans is not reduced even with a bending moment higher than $M_{f,Rd}$. Therefore, modifications were applied to EN1993-1-3 [12] bending-shear interaction equation with aiming to improve the predictions for cold-formed stainless steel LCBs, employing the FE results. It can be also observed that there are two specimens with relatively different behaviour in each set of data corresponding to longer spans, and these specimens are found to be 1 mm thick sections of duplex stainless steel grade 1.4462. This makes these sections the most slender specimens among the considered sections as they have the lowest thickness value of 1 mm and the highest yield stress value of 500 MPa among the considered parameters. Therefore, the influence of local buckling effects could be the reason for relatively lower resistances in these slender sections.

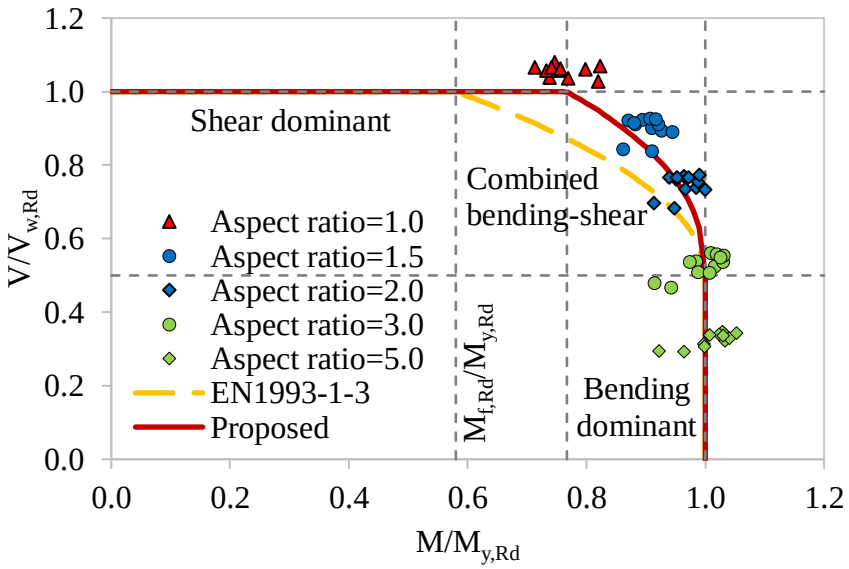

Fig. 12 FE results of stainless steel LCB sections with different aspect ratios against the current and proposed EN1993-1-3 [12] interaction curves

Following the distribution of FE data points and taking into account the effect of bending-shear interaction of LCB sections with aspect ratios of 1.5 and 2.0, EN1993-1-3 [12] interaction equation was modified to the version shown in Eq. (18). When compared to the codified version, the plastic bending resistance of the section ($M_{pl,Rd}$) is replaced with the bending resistance of the section ($M_{y,Rd}$) in this proposed interaction equation and the exponent 2.35 is employed instead of the exponent 2 to redefine the shape of the curve in the bending-shear interaction region. An additional coefficient of 1.3 is introduced to the term bending resistance

consisting of the effective flange area ($M_{f,Rd}$), considering the higher bending moments observed in LCB sections with shorter spans, to redefine the starting point of the bending-shear interaction region.

$$\frac{M_{y,Ed}}{M_{y,Rd}} + \left(1 - \frac{1.3\, M_{f,Rd}}{M_{y,Rd}}\right)\left(\frac{2V_{Ed}}{V_{w,Rd}} - 1\right)^{2.35} \leq 1.0 \quad (18)$$

The comparison of the numerical results with the proposed interaction curve is also shown in Fig. 12. From Fig. 12, it can be seen that there is no reduction in the shear resistance ($V_{w,Rd}$) up to a point closer to the sections with an aspect ratio of 1.0 in the proposed curve. Then, the new curve takes into account the bending and shear interaction of cold-formed stainless steel LCBs up to the location of the sections with an aspect ratio of 3.0 and follows a region of no reduction in cross-section bending resistance ($M_{y,Rd}$). The proposed curve treats the interaction with a curvature and follows well the numerical data points.

Then, a statistical evaluation was conducted for both codified and proposed interaction equations. Tables 14 and 15 present the evaluation results calculated according to Fig. 11 for codified and proposed interaction equations, respectively. The mean and the COV of each case are also given in Tables 14 and 15. Table 14 comprises the sections with aspect ratios of 1.0, 1.5, and 2.0 as these are treated under bending-shear interaction in EN1993-1-3 [12] provisions. However, only the values corresponding to aspect ratios of 1.5 and 2.0 are considered in Table 15 as only these two aspect ratios fall within the proposed interaction region.

Overall, the mean and the COV of numerical to predicted ratio are 1.17 and 0.096, respectively for EN1993-1-3 [12] interaction equation while 1.03 and 0.032, respectively for the proposed interaction equation. The reduced mean and COV of the proposed equation compared to the codified interaction equation imply increased accuracy and consistency of predictions.

560 Table 14 Evaluation of EN1993-1-3 [12] interaction equation according to Fig. 11

LCB section	Aspect ratio=1.0	Aspect ratio=1.5	Aspect ratio=2.0
Stainless steel grade 1.4301			
LCB 150×65×15×1.0	1.28	1.16	1.06
LCB 150×65×15×1.5	1.16	1.12	1.04
LCB 150×65×15×2.0	1.12	1.12	1.04
LCB 200×75×20×1.0	1.40	1.22	1.09
LCB 200×75×20×1.5	1.23	1.18	1.08
LCB 200×75×20×2.0	1.20	1.16	1.08
Stainless steel grade 1.4462			
LCB 150×65×15×1.0	1.34	1.10	0.99
LCB 150×65×15×1.5	1.30	1.16	1.07
LCB 150×65×15×2.0	1.21	1.17	1.08
LCB 200×75×20×1.0	1.44	1.17	1.02
LCB 200×75×20×1.5	1.44	1.23	1.10
LCB 200×75×20×2.0	1.28	1.22	1.12
Mean	1.28	1.17	1.06
COV	0.082	0.036	0.033

561

562

563

564

565

566

567

568

569

570 Table 15 Evaluation of proposed interaction equation for EN1993-1-3 [12] according to Fig. 11

LCB section	Aspect ratio=1.5	Aspect ratio=2.0
Stainless steel grade 1.4301		
LCB 150×65×15×1.0	1.04	1.01
LCB 150×65×15×1.5	1.01	0.99
LCB 150×65×15×2.0	1.03	1.00
LCB 200×75×20×1.0	1.07	1.03
LCB 200×75×20×1.5	1.06	1.02
LCB 200×75×20×2.0	1.04	1.03
Stainless steel grade 1.4462		
LCB 150×65×15×1.0	0.97	0.94
LCB 150×65×15×1.5	1.04	1.01
LCB 150×65×15×2.0	1.05	1.02
LCB 200×75×20×1.0	1.02	0.97
LCB 200×75×20×1.5	1.07	1.04
LCB 200×75×20×2.0	1.08	1.05
Mean	1.04	1.01
COV	0.029	0.029

571

572 ## 6.3 Assessment of SEI/ASCE 8–02 interaction equation

573 SEI/ASCE 8–02 [17] bending-shear interaction equation for the sections with transverse
574 stiffeners was evaluated for cold-formed stainless steel LCB sections utilising the numerical
575 results generated in the parametric study and the assessment details are given in this section.
576 Fig. 13 compares SEI/ASCE 8–02 [17] interaction curve with the FE results from Tables 9-13.
577 From the comparison, it is apparent that the codified interaction equation is too conservative
578 when the V/V_n ratio is closer to 1.0. This is because SEI/ASCE 8–02 [17] interaction equation
579 treats the LCB sections with an aspect ratio of 1.0 within the bending-shear interaction region
580 as similar to EN1993-1-3 [12] interaction equation. Therefore, SEI/ASCE 8–02 [17] interaction
581 equation was modified considering the distribution of the numerical results.

Fig. 13 also includes the circular interaction equation given by Eq. (2) and the rounded interaction equation given by Eq. (3). It can be concluded from the comparison that the circular interaction equation is quite conservative for the bending-shear interaction of cold-formed stainless steel LCB sections. This can be explained by considering the available post-buckling resistance of the LCB sections, which is not taken into account in the circular interaction equation. The rounded interaction equation given by Eq. (3) provides optimised predictions for bending-shear interaction of cold-formed stainless steel LCBs. However, this is also found to be conservative when the V/V_n ratio is closer to 1.0.

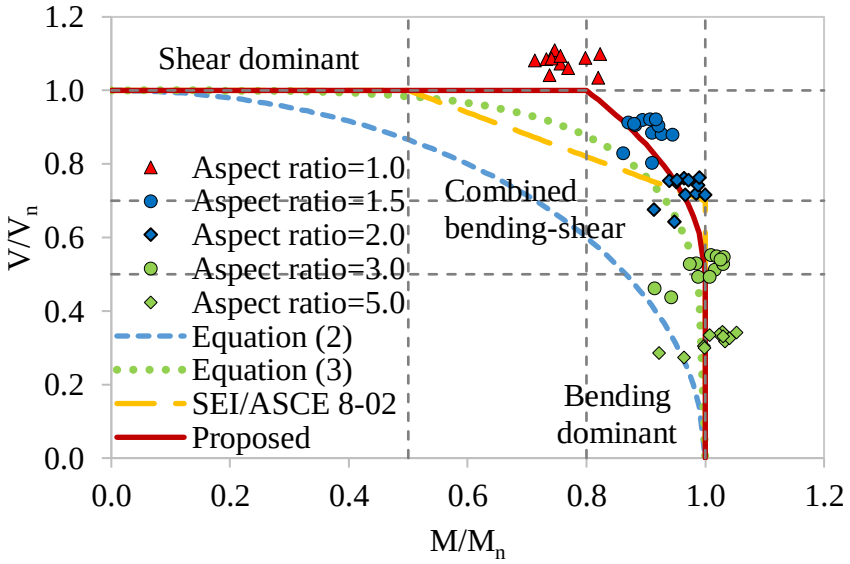

Fig. 13 FE results of stainless steel LCB sections with different aspect ratios against the current and proposed SEI/ASCE 8–02 [17] interaction curves

Considering the bending and shear interaction effect of LCB sections with aspect ratios of 1.5 and 2.0, SEI/ASCE 8–02 [17] interaction equation was modified. The proposed interaction equation for the bending and shear behaviour of cold-formed stainless steel LCB sections is given by Eq. (19). This equation adopts a curved interaction as opposed to SEI/ASCE 8–02 [17] interaction equation and takes into account the bending-shear interaction when the applied bending moment (M) exceeds 80 % of the bending capacity of the section (M_n) and when the applied shear force (V) is greater than half of the section shear capacity (V_n).

$$\left(\frac{M}{M_n}\right) + 0.2\left(\frac{2V}{V_n} - 1\right)^2 \leq 1.0 \text{ for } \frac{M}{M_n} > 0.8 \text{ and } \frac{V}{V_n} > 0.5 \quad (19)$$

Fig. 13 illustrates the comparison of proposed interaction curve with the FE results. It is observed from Fig. 13 that the proposed curve follows well the distribution of the numerical results. Similar to the proposed EN1993-1-3 [12] curve, the proposed SEI/ASCE 8–02 [17] interaction curve also treats the region between the FE data points corresponding to the sections with aspect ratios of 1.0 and 3.0 for the bending-shear interaction of LCB sections.

Then, following a similar approach as discussed in Section 6.2, a statistical evaluation was carried out for both codified and proposed SEI/ASCE 8–02 [17] interaction equations as well. The evaluation results are given in Tables 16 and 17 for the codified and proposed interaction equations, respectively with the mean and the COV of each case. Table 16 includes the results of the sections with aspect ratios of 1.0, 1.5, and 2.0 while Table 17 provides the results for the aspect ratios 1.5 and 2.0, as these fall within the bending-shear interaction regions of the codified and proposed interaction curves, respectively.

From the evaluation, it was found that the codified interaction equation has an overall mean of 1.10 and an overall COV of 0.072 while that for the proposed interaction equation are 1.02 and 0.032, respectively. Therefore, relatively lower mean and COV suggest, improved accuracy and consistency of predictions when using the proposed interaction equation.

627 Table 16 Evaluation of SEI/ASCE 8–02 [17] interaction equation according to Fig. 11

LCB section	Aspect ratio=1.0	Aspect ratio=1.5	Aspect ratio=2.0
Stainless steel grade 1.4301			
LCB 150×65×15×1.0	1.19	1.10	1.02
LCB 150×65×15×1.5	1.16	1.10	1.01
LCB 150×65×15×2.0	1.14	1.10	1.00
LCB 200×75×20×1.0	1.21	1.11	1.01
LCB 200×75×20×1.5	1.17	1.12	1.03
LCB 200×75×20×2.0	1.17	1.12	1.03
Stainless steel grade 1.4462			
LCB 150×65×15×1.0	1.17	1.03	0.94
LCB 150×65×15×1.5	1.20	1.11	1.02
LCB 150×65×15×2.0	1.18	1.13	1.03
LCB 200×75×20×1.0	1.17	1.04	0.93
LCB 200×75×20×1.5	1.23	1.11	1.01
LCB 200×75×20×2.0	1.19	1.13	1.04
Mean	1.18	1.10	1.01
COV	0.018	0.029	0.034

628

629

630

631

632

633

634

635

636

637 Table 17 Evaluation of proposed interaction equation for SEI/ASCE 8–02 [17] according to Fig. 11

LCB section	Aspect ratio=1.5	Aspect ratio=2.0
Stainless steel grade 1.4301		
LCB 150×65×15×1.0	1.01	1.00
LCB 150×65×15×1.5	1.01	0.99
LCB 150×65×15×2.0	1.03	1.00
LCB 200×75×20×1.0	1.04	1.02
LCB 200×75×20×1.5	1.04	1.02
LCB 200×75×20×2.0	1.05	1.04
Stainless steel grade 1.4462		
LCB 150×65×15×1.0	0.95	0.94
LCB 150×65×15×1.5	1.01	1.00
LCB 150×65×15×2.0	1.05	1.02
LCB 200×75×20×1.0	0.98	0.96
LCB 200×75×20×1.5	1.06	1.04
LCB 200×75×20×2.0	1.06	1.05
Mean	1.02	1.01
COV	0.033	0.031

638

639 ## 6.4 Reliability analysis

640 The reliability assessment of the proposed interaction equations was carried out according to
641 Annex D of EN1990 [32] and SEI/ASCE 8-02 [17], and the details are summarised in this
642 section. The material and fabrication uncertainties were given due consideration in the analysis.
643 Afshan et al. [33] proposed statistical data for material parameters to use in reliability
644 calculations in a recent study and these values were adopted in the reliability calculations. The
645 material over-strength factor was taken as 1.3 and 1.1 for austenitic and duplex stainless steel
646 grades, respectively. The values of 0.06 and 0.03 were adopted for the COV of the material
647 strength. The COV of geometric properties was taken as 0.05. Table 18 summarises the key
648 parameters calculated according to EN1990 [32], Annex D to evaluate the reliability of the

proposed EN1993-1-3 [12] interaction equation where b is the mean value correction factor, $k_{d,n}$ is the design fractile factor, V_δ is the coefficient of the variation of the error, and Υ_{M1} is the partial safety factor. The calculated partial safety factor for the proposed interaction equation is less than the recommended value of 1.1 in EN1993-1-4 [11]. The key parameters calculated in the reliability analysis for SEI/ASCE 8-02 [17] are given in Table 19 where P_m and V_P are the mean and the COV of the actual capacity to predicted capacity ratio, respectively, Ø is the resistance factor, and β_0 is the target reliability index. The target reliability index was calculated considering the data for each stainless steel grade separately. From the calculations, both values for target reliability index are found to be greater than the recommended value of 3.0 for structural members in SEI/ASCE 8-02 [17]. Therefore, the proposed interaction equations satisfy the reliability requirements given in Annex D of EN1990 [32] and SEI/ASCE 8-02 [17].

Table 18 Summary of reliability analysis results calculated according to Annex D of EN1990 [32]

	No. of models	b	$k_{d,n}$	V_δ	Υ_{M1}
Proposed EN1993-1-3 interaction [12]	24	1.095	3.56	0.080	1.094

Table 19 Summary of reliability analysis results calculated according to SEI/ASCE 8-02 [17]

Stainless steel grade	No. of models	P_m	V_P	Ø	β_0>3.0
Austenitic	12	1.02	0.018	0.85	3.78
Duplex	12	1.01	0.043	0.85	3.02

7 Concluding remarks

This paper discusses the bending and shear interaction behaviour of cold-formed stainless steel LCB sections which has been given less attention in the past. First, FE models were developed and validated utilising the experimental results found from the literature for cold-formed stainless steel and cold-formed steel. The validation included the comparison of ultimate loads, failure modes and load-deflection curves of three-point and four-point loading tests, and the FE results were found to be agreed well with the experimental results. Then, a comprehensive numerical parametric study was conducted employing the validated FE models to extend the database of cold-formed stainless steel LCBs considering different affecting parameters. This

study comprised 60 FE models of three-point loading simulations of stainless steel LCBs with five different aspect ratios to investigate the shear and bending-shear interaction responses while 12 FE models of four-point bending simulations of stainless steel LCBs to study the bending response. Thereafter, the generated numerical database was analysed for the bending-shear interaction of LCBs.

The diagonal web shear failure was observed in the sections with an aspect ratio of 1.0. Both local buckling of the compression flanges and the diagonal web shear failure occurred in the sections with aspect ratios of 1.5 and 2.0. The local buckling was taken place in the compression flanges of the sections with higher aspect ratios of 3.0 and 5.0. Therefore, it was concluded that the sections with aspect ratios of 1.5 and 2.0 are subjected to bending-shear interaction.

Finally, Eurocode 3 and American specifications interaction equations were evaluated for the bending-shear interaction of cold-formed stainless steel LCB sections using the FE results. It was found that both EN1993-1-3 [12] and SEI/ASCE 8–02 [17] interaction equations are too conservative for a higher level of applied shear force. This is because, the shear resistance of stainless steel LCB sections with shorter spans is not reduced even with a bending moment as high as $1.3 \times M_{f,Rd}$ and this is not taken into consideration in the codified treatment of bending-shear interaction. Therefore, both interaction equations were revised and new interaction equations were proposed using the FE results with aiming to enhance the prediction accuracy. Further, a statistical evaluation was conducted for the proposed interaction equations and assessment of those equations suggested improved and consistent predictions.

Acknowledgements

Authors would like to thank Northumbria University for financial support and providing the necessary research facilities to conduct this research.

References

[1] A. Olsson, Stainless steel plasticity-material modelling and structural applications, PhD thesis, Lulea University of Technology, Sweden, 2001.

[2] E. Real, E. Mirambell, I. Estrada, Shear response of stainless steel plate girders, Eng. Struct. 29 (7) (2007) pp. 1626–1640.

[3] N. Saliba, L. Gardner, Experimental study of the shear response of lean duplex stainless steel plate girders, Eng. Struct. 46 (2013) pp. 375–391.

[4] X. W. Chen, H. X. Yuan, E. Real, X. X. Du, B. W. Schafer, Experimental behaviour of stainless steel plate girders under combined bending and shear, J. Constr. Steel Res. 166 (2020).

[5] F. Sinur, D. Beg, Moment-shear interaction of stiffened plate girders - Tests and numerical model verification, J. Constr. Steel Res. 85 (2013) pp. 116–129.

[6] F. Sinur, D. Beg, Moment-shear interaction of stiffened plate girders - Numerical study and reliability analysis, J. Constr. Steel Res. 88 (2013) pp. 231–243.

[7] P. Keerthan, M. Mahendran, Experimental investigation and design of lipped channel beams in shear, Thin-Walled Struct. 86 (2015) pp. 174–184.

[8] C. H. Pham, G. J. Hancock, Numerical simulation of high strength cold-formed purlins in combined bending and shear, J. Constr. Steel Res. 66 (10) (2010) pp. 1205–1217.

[9] P. Keerthan, M. Mahendran, D. Hughes, Numerical studies and design of hollow flange channel beams subject to combined bending and shear actions, Eng. Struct. 75 (2014) pp. 197–212.

[10] K. Basler, Strength of plate girders under combined bending and shear, J. Struct. Div. 87 (7) (1961) pp. 181–197.

[11] EN 1993-1-4:2006+A1:2015, Eurocode 3 – Design of Steel Structures – Part 1–4: General Rules – Supplementary Rules for Stainless Steels, European Committee for Standardization (CEN), Brussels, 2015.

[12] EN 1993-1-3, Eurocode 3 – Design of steel structures – Part 1–3: General rules – Supplementary rules for cold-formed members and sheeting, European Committee for Standardization (CEN), Brussels, 2006.

[13] EN 1993-1-5, Eurocode 3 – Design of Steel Structures – Part 1–5: Plated Structural Elements, European Committee for Standardization (CEN), Brussels, 2006.

[14] F. Bleich, Buckling Strength of Metal Structures, McGraw Hill, New York, USA, 1952.

[15] F. Shahabian, T. M. Roberts, Behaviour of plate girders subjected to combined bending and shear loading, Scientia Iranica 15 (1) (2008) pp. 16–20.

[16] R. A. LaBoube, W. W. Yu, Cold-formed steel web elements under combined bending and shear, Proceedings of the Fourth International Specialty Conference on Cold-Formed Steel Structures, University of Missouri-Rolla, Missouri, USA, 1978, pp. 219–251.

[17] SEI/ASCE 8–02, Specifications for the Design of Cold-Formed Stainless Steel Structural Members, American Society of Civil Engineers (ASCE), Reston, 2002.

[18] T. Höglund, Behaviour and strength of the web of thin plate I-girders, Bulletin No. 93 of the Division of Building Statics and Structural Engineering, The Royal Institute of Technology, Stockholm, Sweden, 1971, pp. 13–30.

[19] D. M. M. P. Dissanayake, K. Poologanathan, S. Gunalan, K. D. Tsavdaridis, B. Nagaratnam, K. S. Wanniarachchi, Numerical modelling and shear design rules of stainless steel lipped channel sections, J. Constr. Steel Res. (2019) (In press).

[20] AISI S100–16, North American Specification for the Design of Cold-Formed Steel Structural Members, American Iron and Steel Institute (AISI), Washington, 2016.

[21] P. Keerthan, M. Mahendran, Experimental studies on the shear behaviour and strength of LiteSteel beams, Eng. Struct. 32 (10) (2010) pp. 3235–3247.

[22] P. Keerthan, M. Mahendran, Shear behaviour and strength of LiteSteel beams with web openings, Adv. Struct. Eng. 15 (2) (2012) pp. 171–184.

[23] M. Mahendran, P. Keerthan, Experimental studies of the shear behavior and strength of LiteSteel beams with stiffened web openings, Eng. Struct. 49 (2013) pp. 840–854.

[24] R. Siahaan, M. Mahendran, P. Keerthan, Section moment capacity tests of rivet fastened rectangular hollow flange channel beams, J. Constr. Steel Res. 125 (2016) pp. 252–262.

[25] I. Arrayago, E. Real, L. Gardner, Description of stress-strain curves for stainless steel alloys, Mater. Des. 87 (2015) pp. 540–552.

[26] S. Niu, K. J. R. Rasmussen, F. Fan, Distortional-global interaction buckling of stainless steel C-beams: Part II - Numerical study and design, J. Constr. Steel Res. 96 (2014) pp. 40–53.

[27] P. Keerthan, M. Mahendran, New design rules for the shear strength of LiteSteel beams, J. Constr. Steel Res. 67 (6) (2011) pp. 1050–1063.

[28] L. Gardner, D. A. Nethercot, Numerical modeling of stainless steel structural components—A consistent approach, J. Struct. Eng. 130 (10) (2004) pp. 1586–1601.

[29] P. Keerthan, M. Mahendran, Numerical modeling of LiteSteel beams subject to shear, J. Struct. Eng. 137 (12) (2011) pp. 1428–1439.

[30] P. Keerthan, M. Mahendran, Shear buckling characteristics of cold-formed steel channel beams, Int. J. Steel Struct. 13 (3) (2013) pp. 385–399.

[31] P. Keerthan, M. Mahendran, Improved shear design rules of cold-formed steel beams, Eng. Struct. 99 (2015) pp. 603–615.

[32] EN 1990:2002+A1:2005, Eurocode – Basis of Structural Design, European Committee for Standardization (CEN), Brussels, 2005.

771 [33] S. Afshan, P. Francis, N. R. Baddoo, L. Gardner, Reliability analysis of structural
772 stainless steel design provisions, J. Constr. Steel Res. 114 (2015) pp. 293–304.